Shape Distributions for Gaussian Molecules: Circular and Linear Chains in Two Dimensions

L. Y. Shy and B. E. Eichinger*

Department of Chemistry, University of Washington, Seattle, Washington 98195.
Received August 5, 1985

ABSTRACT: The shape distribution functions $P(\tilde{S}_1,\tilde{S}_2)$ for the principal components of the gyration tensors for Gaussian molecules in 2-dimensional space have been numerically evaluated for both circular and linear chains. It is found that the most probable configurations are quite compact in comparison with the mean squared dimensions. Fluctuations away from the most probable configurations are achieved primarily by extension in one direction only, rather than by a uniform inflation. The theory for disks is given, and these distribution functions are also evaluated. Although disks are improbable when compared with all ellipsoids, their distributions may be formulated on appropriate subspaces. They complete the description of two-dimensional configurations.

Introduction

The distribution of configurations for polymer molecules is of primary importance in the theory of solution thermodynamics and can have a general influence on our perception of the shape of randomly coiling molecules. Investigations[1-3] of distribution functions of the squared radii of gyration have yielded much information on the size of molecules. However, the analysis of the distributions of the principal components of the radii of gyration of molecules has encountered considerable difficulties. Monte Carlo methods provide reasonable estimates of the general features of distributions for various models[4-7] of linear chains, but this method soon becomes intractable if the molecular connectivity is more complicated than that for a linear chain.

Recently, we have formulated a general solution[8] to the shape distribution problem for Gaussian molecules of arbitrary connectivity with use of the theory of multivariate statistics. The method is more direct than the earlier treatment,[9,10] and it is adaptable to various structures through specification of a Kirchhoff matrix that describes molecular connectivity. It is hoped that the lessons we learn from solving the equations for linear and circular chains will eventually apply to the theory of rubber elasticity,[11-13] besides being of interest in their own right.

In this contribution, all configurations of interest are in 2-dimensional space. We first numerically evaluate the distribution functions for both circular and linear chains. Then the theory for disks is discussed, and their distributions are computed.

Circular Chain (Elliptical Configurations)

When an appropriate change of variables is made, the shape distribution[8] for the two-dimensional circular chain with an odd number n of beads may be written as

$$P_n(\tilde{S}_1,\tilde{S}_2) = -\tilde{\Delta}\sum_{j>k}^{(n-1)/2}\sum B_jB_k(\kappa_j-\kappa_k)\exp[-(\kappa_j-\kappa_k)\tilde{s}^2/2]\int_0^{2(\tilde{S}_1\tilde{S}_2)^{1/2}}dx\,\frac{\sinh[(1/2)(\kappa_j-\kappa_k)(\tilde{\Delta}^2+x^2)^{1/2}]}{(\tilde{\Delta}^2+x^2)^{1/2}} \quad (1)$$

where the variables $\tilde{s}^2$, $\tilde{\Delta}$, κ_j, and B_j are defined by

$$\tilde{s}^2 = \tilde{S}_1 + \tilde{S}_2$$

$$\tilde{\Delta} = \tilde{S}_1 - \tilde{S}_2$$

$$\kappa_j = n^2\lambda_j$$

$$B_j = \kappa_j/\prod_{m\neq j}(1-\kappa_j/\kappa_m)$$

The reduced variables $\tilde{S}_\alpha = \gamma S_\alpha/n$, with $\gamma = 1/\langle l^2\rangle_0$, are introduced so that $P_n(\tilde{S}_1,\tilde{S}_2)\,d\tilde{S}_1\,d\tilde{S}_2$ converges to $P_\infty(\tilde{S}_1,\tilde{S}_2)\,d\tilde{S}_1\,d\tilde{S}_2$ as $n\to\infty$. The λ_j are the eigenvalues of the Kirchhoff-Rouse-Zimm matrix,[14] and $\langle l^2\rangle_0$ is the mean-square segment length.

The probability distribution $P_5(\tilde{S}_1,\tilde{S}_2)$ evaluated by the subroutine DCADRE[15] is shown in Figure 1. In the figure, $P_5(\tilde{S}_1,\tilde{S}_2)$ is plotted against $\tilde{S}_1$ and $\tilde{S}_2$ with the same grid size for both abscissae (0.005 for this case). As required by eq 1, $P_n(\tilde{S}_1,\tilde{S}_2)$ should have null probability for $\tilde{S}_1 \le \tilde{S}_2$. This feature is apparent on close inspection, in spite of the fact that the graphics software has drawn the grids unequally. The probability that the molecule is a disk, with $\tilde{S}_1 = \tilde{S}_2$, is zero when measured in the space of all elliptical configurations. A nontrivial probability for disks is only obtainable upon constraining the configurations, as will be seen later. For this short chain, the most probable configuration (denoted by a prefixed asterisk) is a highly anisometric rodlike shape, with $^*\tilde{S}_1 \simeq 0.030$ and $^*\tilde{S}_2 \simeq 0.005$. For $n = 49$ (Figure 2a), the ellipse with $^*\tilde{S}_1 \simeq 0.033$ and $^*\tilde{S}_2 \simeq 0.015$ is most probable. The most probable squared radius of gyration $^*\tilde{s}^2 = {}^*\tilde{S}_1 + {}^*\tilde{S}_2 \simeq 0.048$ is a mere 58% of the mean squared dimension $\langle s^2\rangle_0$ ($^1/_{12} \simeq 0.083$), with the components being 40% and 18% of $\langle s^2\rangle_0$, respectively. The location of the extremum in relation to $\langle s^2\rangle_0$ is more apparent in Figure 2b, which is the same surface as Figure 2a but viewed from a different angle. The most striking feature of these distributions is their long tails as $\tilde{S}_1$ becomes large. Although the molecules are likely to be quite compact, the fluctuations that occur are highly asymmetric. They are apt to have a breadth near $\tilde{S}_2 \simeq 0.015$ (the ridge seen in Figure 2b) and to expand and contract primarily along the larger principal component axis. This axis is not oriented on the plane but has a random direction if the molecules are free of additional constraints.

The shape distribution of two-dimensional rings has been addressed previously by Šolc and Gobush.[10] Their results, depicted as asymmetry distributions,[10] cannot be compared directly with these calculations. Instead, comparisons can be made for ratios of the asymmetry distribution with our presentation. Good agreement with the Šolc and Gobush calculations has been found for both $n = 5$ and $n = 49$.

The asymptotic distribution for linear chains has been given,[8] but that for rings has not. To obtain the distribution for large values of $\tilde{S}_1$ one requires an estimate of the integral in eq 1, which may be accomplished by series expansion of the hyperbolic sine function with term-by-term integration, to give the integral, called $I(\tilde{s}^2,\tilde{\Delta})$, as

$$I(\tilde{s}^2,\tilde{\Delta}) = \sum_{n=0}^{\infty}\frac{(\beta\tilde{\Delta})^{2n+1}}{(2n+1)!}\sum_{k=0}^{n}\binom{n}{k}\frac{[2(\tilde{S}_1\tilde{S}_2)^{1/2}/\tilde{\Delta}]^{2k+1}}{2k+1} \quad (2)$$

0024-9297/86/2219-0838$01.50/0

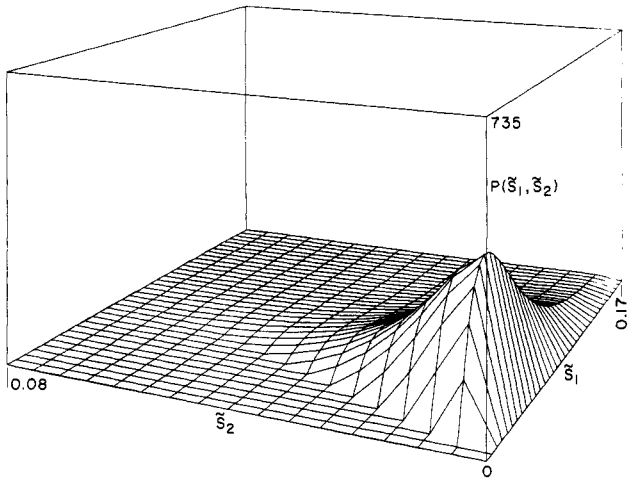

Figure 1. The shape distribution function $P_5(\tilde{S}_1,\tilde{S}_2)$ for the circular chain with 5 beads. The reduced principal components of the gyration tensor $\tilde{S}_i$ are defined by $S_i/n\langle l^2\rangle_0$, where $\langle l^2\rangle_0$ is the unperturbed dimension of a segment.

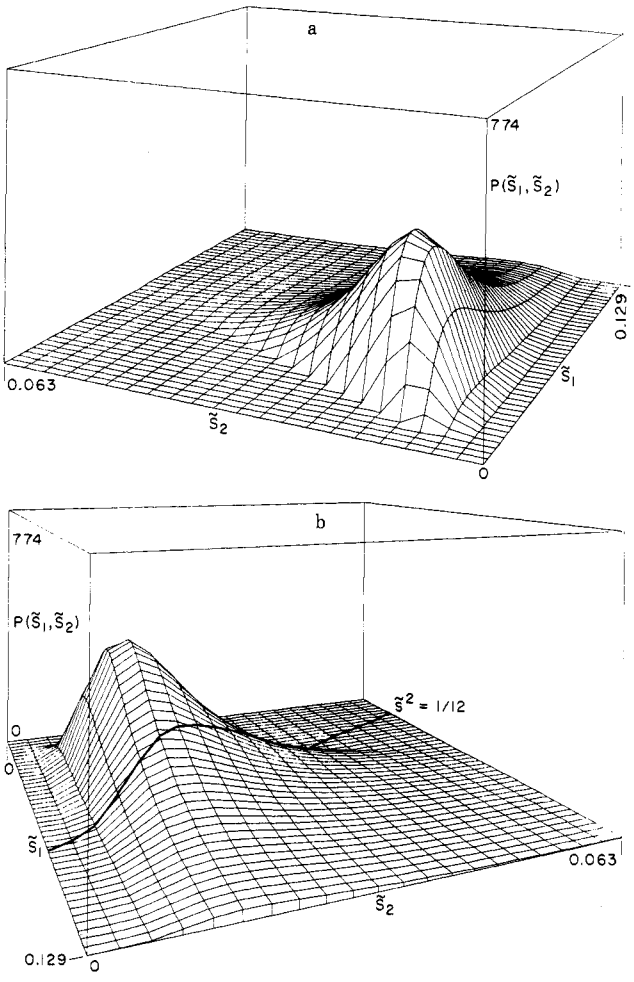

Figure 2. (a) The distribution function for circular chains with $n = 49$. (b) Another view of Figure 2a. The heavy line depicts the mean squared radius of gyration $\langle \tilde{s}^2\rangle = {}^1/_{12}$ for the circular chain.

If the most probable configurations for large $\tilde{s}^2$ are highly asymmetric, as computations aver, then $(\tilde{S}_1\tilde{S}_2)^{1/2}/\tilde{\Delta}$ is a small quantity and the first term in the inner sum of eq 2 gives the asymptotic value of the integral. Thus, we have

$$I(\tilde{s}^2,\tilde{\Delta}) \sim 2(\tilde{S}_1\tilde{S}_2)^{1/2}\tilde{\Delta}^{-1}\sinh(\beta\tilde{\Delta})$$

and

$$P_\infty(\tilde{S}_1,\tilde{S}_2)\,d\tilde{S}_1\,d\tilde{S}_2 \sim -(\lambda_2-\lambda_1)B_1B_2(\tilde{S}_1\tilde{S}_2)^{1/2}\exp[-(\lambda_1\tilde{S}_1+\lambda_2\tilde{S}_2)]\,d\tilde{S}_1\,d\tilde{S}_2 \quad (3)$$

which differs from the linear chain result (eq 29 of ref 8) in the important respect that $(\tilde{S}_1\tilde{S}_2)^{1/2}$ (ring) stands in place of $|\tilde{S}_1^{-1}-\tilde{S}_2^{-1}|^{1/2}$ (linear).

The most probable of the highly extended configurations of the linear chain are those with $\tilde{S}_2 \to 0$. However, for circular chains the most probable value for $\tilde{S}_2$ when $\tilde{S}_1$ is a fixed large number is $1/2\kappa_2$, or $S_2/n\langle l^2\rangle_0 = \tilde{S}_2 \simeq 1/32\pi^2$ for large n. The circular chain is constrained by its topology to have a greater breadth than the linear chain in the asymptotic region. It is again gratifying to see that the Gaussian model bears some resemblance to reality.

Linear Chain (Elliptical Configurations)

For the purposes of calculation it is convenient to write $P_n(\tilde{S}_1,\tilde{S}_2)$ in the form[8]

$$P_n(\tilde{S}_1,\tilde{S}_2) = (\tilde{\Delta}/\pi)|-i\kappa|\int_0^\infty x_-J_0(\tilde{\Delta}x_-)\,dx_- \times \int_{-\infty}^{\infty}\frac{\exp(i\tilde{s}^2x_+)\,dx_+}{\prod_{m=1}^{n-1}(x_+ + x_- - i\kappa_m)^{1/2}(x_+ - x_- - i\kappa_m)^{1/2}} \quad (4)$$

Here $|-i\kappa| = \prod(-i\kappa_m)$, and $J_0(\tilde{\Delta}x_-)$ is the Bessel function of the first kind of order zero. There are $n-1$ pairs of branch points in the second integral at

$$x_+ = \pm x_- + i\kappa_m \qquad (m = 1, 2, ..., n-1)$$

One may choose to connect each pair of these points with a horizontal branch cut and replace the above integral by the sum of integrals along the cuts. That is

$$\int_{-\infty}^{\infty}\frac{\exp(i\tilde{s}^2x_+)\,dx_+}{\prod_m(x_+ + x_- - i\kappa_m)^{1/2}(x_+ - x_- - i\kappa_m)^{1/2}} = \sum_{j=1}^{n-1}\oint_{\mathrm{cut}j}\frac{\exp(i\tilde{s}^2x_+)\,dx_+}{\prod_m(x_+ + x_- - i\kappa_m)^{1/2}(x_+ - x_- - i\kappa_m)^{1/2}}$$

Letting $x_+ = i\kappa_j + t$, we immediately have

$$P_n(\tilde{S}_1,\tilde{S}_2) = \frac{\tilde{\Delta}}{\pi}|-i\kappa|\int_0^\infty x_-J_0(\tilde{\Delta}x_-)\,dx_- \times \oint\sum_j\frac{\exp(-\tilde{s}^2\kappa_j)\exp(i\tilde{s}^2t)\,dt/(t^2-x_-^2)^{1/2}}{\prod_{m\neq j}[t+x_-+i(\kappa_j-\kappa_m)]^{1/2}[t-x_-+i(\kappa_j-\kappa_m)]^{1/2}} \quad (5)$$

The complex t plane is mapped onto the w plane while opening the cut on the real axis by the transformation[16] $t = (x_-/2)(w + w^{-1})$. The transformation is forced to be single valued by opting to map the part of the t plane that is off the cut on the real axis to the outside of the unit disk on the w plane. Thus, one has

$$dt/(t^2-x_-^2)^{1/2} = \pm dw/w$$

The contour around the cut now encloses a single pole at $w = 0$ and hence may be shrunk to the circumference of the unit disk in the w plane. That is, $w = e^{i\theta}$ and $dw = iw\,d\theta$; take the positive sign in the denominator to get

$$P(\tilde{S}_1,\tilde{S}_2) = (i\tilde{\Delta}/\pi) \times |-i\kappa|\int_0^\infty x_-J_0(\tilde{\Delta}x_-)\,dx_-\sum_j\exp(-\tilde{s}^2\kappa_j)\int_0^{2\pi}H_j(\tilde{s}^2,x_-,\theta)\,d\theta \quad (6)$$

where $H_j(\tilde{s}^2,x_-,\theta)$ is defined as

$$H_j(\tilde{s}^2,x_-,\theta) = \exp(i\tilde{s}^2x_-\cos\theta)/\{\prod_{m\neq j}[x_-(\cos\theta+1)+i(\kappa_j-\kappa_m)]^{1/2}[x_-(\cos\theta-1)+i(\kappa_j-\kappa_m)]^{1/2}\} \quad (7)$$

This may be further reduced to

$$P(\tilde{S}_1,\tilde{S}_2) = \frac{2\tilde{\Delta}(-1)^{1+[n/2]}}{\pi}|\kappa|\int_0^\infty x_- J_0(\tilde{\Delta}x_-)\,dx_- \int_0^\pi d\theta \times \sum_j^{n-1} \exp(-\kappa_j\tilde{s}^2)(\substack{\text{Real}\\\text{Imag}})H_j(\tilde{s}^2,x_-,\theta) \quad (8)$$

where the real part is taken for even n and the imaginary part for odd n, and $[n/2]$ is the integer part of $n/2$.

In the numerical evaluation of eq 8, care must be taken with the standard computer software to ensure that the branch cut of the square root functions are handled properly. It is first of all imperative that the roots be computed before the product to avoid an uncontrolled passage over a cut. To ensure that the code is working properly, it is useful to plot the computed value of the integrand of eq 4 on the x_+ complex plane. We have done this (not shown) to convince ourselves that the code is correct.

The evaluation of eq 8 by a double integral subroutine proved to be inefficient. The alternative is to first integrate over θ at appropriate grid points ($\tilde{s}^2$, x_-). The resulting integrand was then interpolated with use of the Lagrangian five-point formula[17] to accomplish the second integral.

The probability distributions $P_n(\tilde{S}_1,\tilde{S}_2)$ for $n = 5$ and $n = 49$ are displayed in Figures 3 and 4. These have the same general characteristics as those found for the circular chain with some important difference in detail. For example, both the linear and circular chains are highly asymmetric in the extended region, but the linear chain has a higher probability for extended configurations than does the circular, as stands to reason. Furthermore, the most probable configuration is larger than that for the circular chain, but in relation to the mean-squared radii of gyration it is smaller. For $n = 49$, $^*\tilde{S}_1$ and $^*\tilde{S}_2$ are found to be 0.048 and 0.018, with $^*\tilde{s}^2$ being only 40% of the mean square radius of gyration, $\langle s^2\rangle_0 = {}^1/_6$. Calculations made for a longer chain ($n = 99$) verify that $n = 49$ is essentially at the asymptotic limit, at least within the numerical precision of these results. The most probable configurations for both circular and linear chains of various lengths are tabulated in Table I.

The validity of the above calculations was further checked by integrating $P_n(\tilde{S}_1,\tilde{S}_2)$ over $\tilde{\Delta}$ to give $P_n(\tilde{s}^2)$ through the equation

$$P_n(\tilde{s}^2) = (1/2)\int_0^{\tilde{s}^2} P(\tilde{S}_1,\tilde{S}_2)\,d\tilde{\Delta} \quad (9)$$

This result is then compared with that calculated directly[18] from $P_n(\tilde{s}^2)$

$$P_n(\tilde{s}^2) = (1/2\pi)\int_{-\infty}^{\infty} \frac{\exp(i\beta\tilde{s}^2)}{\prod_{m=1}^{n-1}(1 + i\beta/\kappa_m)}\,d\beta \quad (10)$$

The comparison is made in Figure 5 for $n = 49$. The two curves are indistinguishable except at large $\tilde{s}^2$. In this region, $J_0(\tilde{\Delta}x_-)$ oscillates very rapidly, and a grid size for x_- that varies inversely as $\tilde{\Delta}$ would be required to interpolate the integrand with uniform precision. This was not done for the calculations that are reported in Figure 4. It will be noted that the discrepancy in Figure 5 occurs for larger values of $\tilde{s}^2$ than are depicted in the truncated Figure 4.

Symmetric Configurations

The previous treatment of ellipsoids of revolutions[8] that was produced by the second named author of this paper is in error, and we would like to take this opportunity to

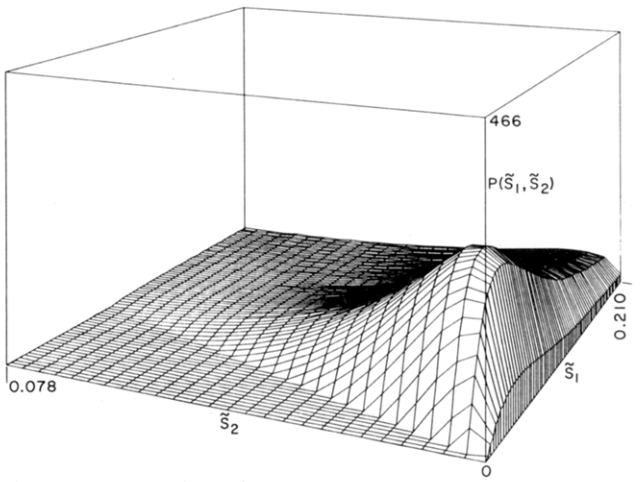

Figure 3. The distribution function for the elliptical configurations of the linear chain with 5 beads.

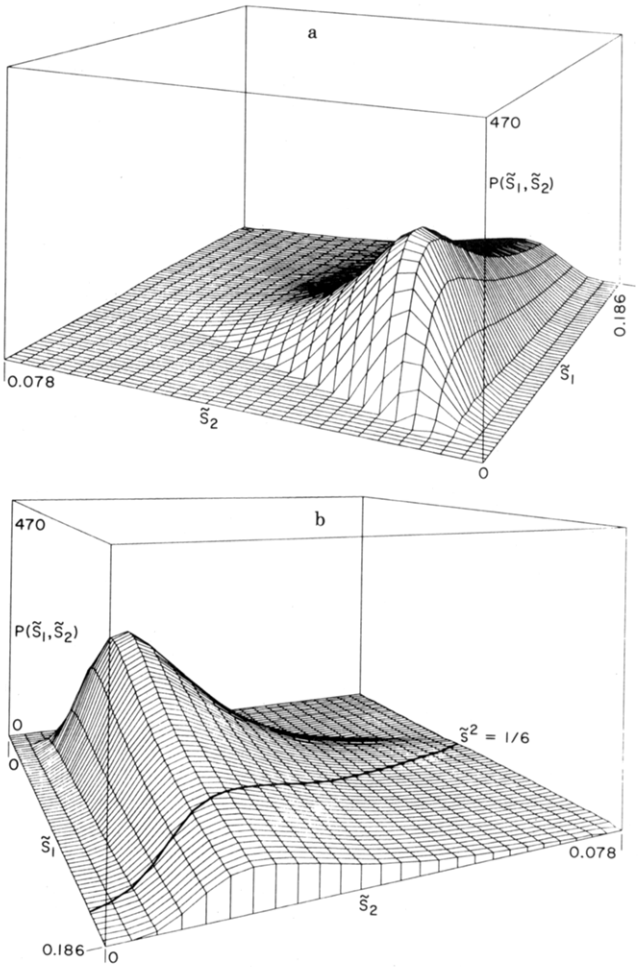

Figure 4. (a) The distribution function for linear chains of $n = 49$ beads. Otherwise the same as Figure 3. (b) Another view of Figure 4a. The heavy curve locates the mean squared radius of gyration, $\langle\tilde{s}^2\rangle = {}^1/_6$.

Table I
Most Probable Configurations (Ellipses)

n	grid size	$^*\tilde{S}_1$	$^*\tilde{S}_2$	probability
		Circular		
5	0.005	0.030	0.005	372.75
49	0.003	0.033	0.015	499.80
		Linear		
5	0.003	0.045	0.006	258.04
49	0.003	0.048	0.018	306.13
99	0.003	0.048	0.018	305.06

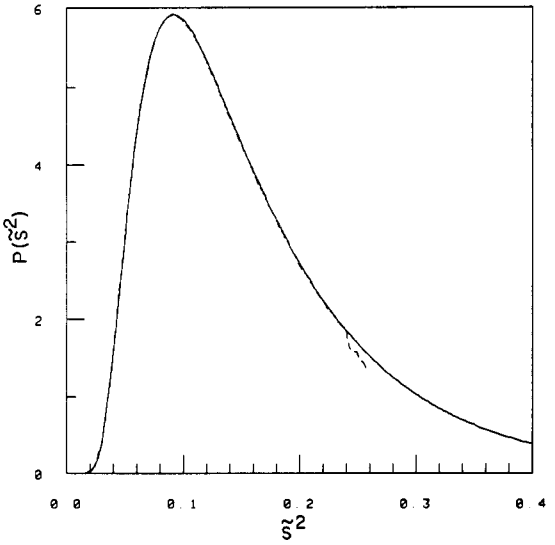

Figure 5. The distribution of the squared radius of gyration $\tilde{s}^2$ for a linear chain with $n = 49$. The dashed curve results from integrating $P_{49}(\tilde{S}_1,\tilde{S}_2)\,d\tilde{S}_1\,d\tilde{S}_2$ along contours of constant $\tilde{s}^2$. The solid curve is calculated directly from eq 10.

correct the mistake for the general case before applying the result to the probability distribution for disks. We begin with eq 24 of ref 8, which, with a minor change of notation, gives the metric on the $k(n-1)$ dimensional normal mode space $\mathbf{Q}_0 = h\sigma\mathbf{V}$ as

$$d\xi^2 = \sum_{\alpha=1}^{k} d\sigma_\alpha{}^2 + 2\sum_{\alpha<\beta}[(\sigma_\alpha - \sigma_\beta)^2\delta\theta_{\alpha\beta}{}^2 + (\sigma_\alpha + \sigma_\beta)^2\delta\phi_{\alpha\beta}{}^2] + \sum_{\alpha=1}^{k}\sigma_\alpha{}^2\sum_{j=1}^{n-k-1}\delta v_{2,\alpha j}{}^2 \quad (11)$$

Now, if the class of configurations of interest has some symmetry so that two or more of the σ_α are equal to one another, some of the $\delta\theta_{\alpha\beta}$ will not appear in $d\xi^2$. This has been the source of confusion that motivated the incorrect formulation of the problem.

There is nothing wrong with eq 11 for symmetric configurations. The matrices $\delta\theta$ and $\delta\phi$ are two copies of the components of the metric on $SO(k)$. When transforming back to the components of $\mathbf{V} \sim SO(k) \times SO(n-1)/SO(k) \times SO(n-k-1)$ and $h \sim SO(k)$, one need only note that the missing $\delta\theta_{\alpha\beta}$ correspond to the subgroup of $SO(k)$ that commutes with the diagonal and degenerate matrix σ.

An illustration may be in order. An arbitrary configuration of four points in three space has $4 \times 3 = 12$ degrees of freedom: three of these are translational (hence deleted), leaving nine in the normal coordinates $\mathbf{Q}_0 = h\sigma\mathbf{V}$. There are three variables in $h \sim SO(3)$, three in σ, and three in $\mathbf{V} \sim SO(3)$. Now suppose that the configuration becomes a regular tetrahedron, so that σ is a multiple of the unit matrix. Then h and $\mathbf{V}$ both commute with σ, and $\mathbf{Q}_0 \rightarrow \sigma\, h\mathbf{V} = h\mathbf{V}\sigma$. But $h \sim SO(3)$ and $\mathbf{V} \sim SO(3)$, so that $h\mathbf{V} \sim SO(3)$ by the fundamental property of groups. We are left with only four degrees of fredom: the one unique component of σ (proportional to the edge length of the regular tetrahedron) and the three components of $\phi \sim h\mathbf{V}$ (corresponding to rigid-body rotations). It is of some interest here that the rigid-body rotations contained in the elements of h and the pseudorotations contained in $\mathbf{V}$ are indistinguishable from one another in this case.

On inspection of the general case, it is found that one may make an arbitrary decision as to the identity of the components of the rotation matrices that are absent when σ has m equal components. It is convenient to keep the components of $\mathbf{V}$ intact and to let those of h disappear. The polar decomposition $\mathbf{Q}_0 = h\sigma\mathbf{V}$ then consists of $h \sim SO(k)/SO(m)$, $\sigma \sim W^{k-m+1}$, and $\mathbf{V} \sim SO(n-1)/SO(n-k-1)$. The count of variables is $h = (k-m)(k+m-1)/2$, $\sigma = k-m+1$, $\mathbf{V} = k(n-1) - k(k+1)/2$, total $= k(n-1) - (m+2)(m-1)/2$.

At this stage the secure procedure is to formulate the distribution function problem in Eckart coordinates, use the δ function to ensure $\mathbf{V}\mathbf{V}' = \mathbf{1}_k$, and make an appropriate change of variables to obtain an equation having a structure similar to eq 4. For present purposes we shall do this for disks, i.e., for $\sigma = (nS)^{1/2}\mathbf{1}_2$, with the squared radius of gyration $s^2 = 2S$.

Equation 11 gives

$$d\xi^2 = (n/2S)(dS)^2 + 8nS\delta\phi_{12}{}^2 + nS\sum_{\alpha=1}^{2}\sum_{j=1}^{n-3}\delta v_{2,\alpha j}{}^2$$

and the corresponding volume element is

$$d\mathbf{Q}_0 = (\text{const})n^{n-2}S^{n-3}\,dS\,d\mathbf{V} \quad (12)$$

Since we have not yet been able to normalize the distribution function by direct integration, the "const" in eq 12 will be absorbed into the overall normalization.

The probability distribution for disks is now given by

$$P(S)\,dS = C_0{}^{-1}S^{n-3}\,dS\int_{SO(n-1)/SO(n-3)}\text{etr}\,(-\gamma nS\mathbf{V}\Lambda_0\mathbf{V}')\,d\mathbf{V}$$

where

$$C_0 = \int_0^\infty S^{n-3}\,dS\int_{SO(n-1)/SO(n-3)}\text{etr}\,(-\gamma nS\mathbf{V}\Lambda_0\mathbf{V}')\,d\mathbf{V}$$

To remove the restriction on $\mathbf{V}$, insert δ functions to obtain

$$P(S)\,dS = (2\pi)^{-3}C_0{}^{-1}S^{n-3}\,dS\int_{R^3}d\mathbf{k}\int_{R^{2(n-1)}}\text{etr}\,(i\mathbf{k} - i\mathbf{k}\mathbf{V}\mathbf{V}')\,\text{etr}\,(-\gamma nS\mathbf{V}\Lambda_0\mathbf{V}')\,d\mathbf{V} = (2\pi)^{-3}C_0{}^{-1}S^{n-3}\,dS \times \int_{R^3}d\mathbf{k}\,\text{etr}\,(i\mathbf{k})|\gamma nS\mathbf{1}_2 \otimes \Lambda_0 + i\mathbf{k} \otimes \mathbf{1}_{n-1}|^{-1/2}$$

Here

$$k = \begin{bmatrix} k_{11} & (1/2)k_{12} \\ (1/2)k_{12} & k_{22} \end{bmatrix}$$

and $d\mathbf{k} = dk_{11}\,dk_{22}\,dk_{12}$. The volume element $d\mathbf{k}$ in the polar coordinates

$$k = \begin{bmatrix} \cos\theta & \sin\theta \\ -\sin\theta & \cos\theta \end{bmatrix}\begin{bmatrix} k_1 & 0 \\ 0 & k_2 \end{bmatrix}\begin{bmatrix} \cos\theta & -\sin\theta \\ \sin\theta & \cos\theta \end{bmatrix}$$

is $d\mathbf{k} = 2|k_1 - k_2|\,dk_1\,dk_2\,d\theta$. The integral on θ is trivial, leaving

$$P(S)\,dS = (2\pi^2)^{-1}C_0{}^{-1}S^{n-3}\,dS\int_{-\infty}^{\infty}dk_1 \times \int_{-\infty}^{k_1}dk_2\,\frac{\exp[i(k_1+k_2)]|k_1-k_2|}{\prod_{\alpha=1}^{2}\prod_{m=1}^{n-1}(\gamma nS\lambda_m + ik_\alpha)^{1/2}}$$

Now define $\tilde{S} = \gamma S/n$, $k_\alpha = \tilde{S}x_\alpha$, and $\kappa_m = n^2\lambda_m$ as before, so that

$$P_n(\tilde{S})\,d\tilde{S} = C_2{}^{-1}\tilde{S}\,d\tilde{S}\int_{-\infty}^{\infty}dx_1\int_{-\infty}^{x_1}dx_2\,\frac{\exp[i(x_1+x_2)\tilde{S}]|x_1-x_2|}{\prod_{\alpha=1}^{2}\prod_{m=1}^{n-1}(\kappa_m + ix_\alpha)^{1/2}} \quad (13)$$

This will be recognized as equivalent to eq 4 with the argument of the Bessel function set to zero and with the

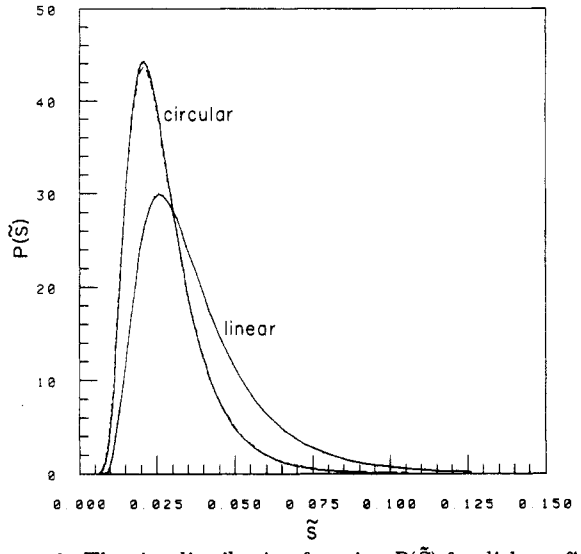

Figure 6. The size distribution function $P(\tilde{S})$ for disk configurations. Curves to the left are for circular chains and those on the right are for linear chains. Symbols: dash, $n = 29$; solid $n = 49$; point, $n = 71$ (the solid curve and points are indistinguishable at this resolution).

appropriate modification of $|\tilde{S}_1 - \tilde{S}_2|\, d\tilde{S}_1\, d\tilde{S}_2$ for the degenerate case that $\tilde{S}_1 = \tilde{S}_2 = \tilde{S}$.

Numerical Evaluation for Disk Configurations

To make eq 13 more amenable to computation, let $x_+ = x_1 + x_2$, $x_- = x_1 - x_2$, and $C = C_2|\kappa|$ to obtain

$$P_n(\tilde{S})\, d\tilde{S} = 2^{n-2}C^{-1}|-i\kappa|\tilde{S}\, d\tilde{S} \int_0^\infty x_-\, dx_- \times \int_{-\infty}^{\infty} \frac{\exp(ix_+\tilde{S})x_+\, dx_+}{\prod_{m=1}^{n-1}(x_+ + x_- - i2\kappa_m)^{1/2}(x_+ - x_- - i2\kappa_m)^{1/2}} \quad (14)$$

For circular chains with an odd number of bonds the residue theorem may be used to reduce eq 14 to

$$P_n(\tilde{S})\, d\tilde{S} = (2\pi i)C^{-1}|-i\kappa|^2\tilde{S}\, d\tilde{S} \sum_j \frac{\exp(-2\tilde{S}\kappa_j)}{\prod_{m\neq j} i(\kappa_j - \kappa_m)} \int_0^\infty [F_j(x) - F_j(-x)] \quad (15)$$

Here $F_j(x)$ and $|-i\kappa|$ are defined by

$$F_j(x) = \frac{\exp(ix\tilde{S})}{\prod_{m\neq j}^{(n-1)/2} [x + i(\kappa_j - \kappa_m)]}$$

$$|-i\kappa| = \prod_{m=1}^{(n-1)/2} (-i\kappa_m)$$

The integral could be expressed as an exponential integral, but we prefer a different reduction. Since $F_j(-x) = (-1)^{[(n-1)/2]-1}\bar{F}_j(x)$, eq 15 becomes

$$P_n(\tilde{S})\, d\tilde{S} = 4\pi C^{-1}(-1)^{[[n-1]/4]}|\kappa|\tilde{S}\, d\tilde{S} \sum_j B_j \times \exp(-2\tilde{S}\kappa_j) \int_0^\infty ({}^{\text{Real}}_{\text{Imag}})F_j(x) \quad (16)$$

This was evaluated by Romberg's extrapolation method[19] with the integrand at the upper limit being no more than 0.1% of the extremum. The size distributions $P_n(\tilde{S})$ for circular chains with $n = 29$, 49, and 71 are illustrated in Figure 6. The weak chain length dependence of $P_n(\tilde{S})$ indicates that for our purposes the distributions for these n are indistinguishable from that for the asymptotic limit; they give the most probable configuration at $^*\tilde{S} = 0.0205$ and averaged dimension $\langle\tilde{S}\rangle = 0.0275$. The relatively small value of $^*\tilde{S}$ is interesting in comparison with the region of the elliptical distribution that is most nearly circular. Note that $^*\tilde{S}$(disk) is close to $^*\tilde{S}_2$ for the elliptical configuration (0.015). The $\tilde{S}_1$ axis is evidently compressed as the ellipse is squeezed into a disk, while $\tilde{S}_2$ expands relatively little. A close examination of Figure 2a indicates that as one moves off the line $\tilde{S}_1 = \tilde{S}_2$, the probability distribution function for ellipses is very steep in the direction leading from the point $^*\tilde{S} = \tilde{S}_1 = \tilde{S}_2$ up to the most probable configuration. That is, the elliptical configurations that are most nearly disks are also close to the most probable disk. This concurrence supports the accuracy of the calculations.

Table II
Most Probable Configurations (Disks)

n	grid size	$^*\tilde{S}$	probability	C^a	$\langle\tilde{S}\rangle$
			Circular		
29	0.0005	0.0205	43.64	537.84	0.0275
49	0.0005	0.0205	44.13	549.90	0.0276
71	0.0005	0.0205	44.20	553.42	0.0275
			Linear		
49	0.0015	0.0255	29.95	206.10	0.0376
71	0.0015	0.0255	30.11	206.42	0.0374

[a] Value of the normalization constant in eq 16 or 17.

For the case of linear chains, eq 16 is reminiscent of eq 4 for the elliptical probability distribution. One may apply the procedure used for that equation to obtain

$$P_n(\tilde{S})\, d\tilde{S} = C^{-1}(-1)^{1+[n/2]}\tilde{S}\, d\tilde{S} \int_0^\infty x_-\, dx_- \int_0^\pi d\theta \sum_{j=1}^{n-1}(2\kappa_j) \times \exp(-2\kappa_j\tilde{S})({}^{\text{Real}}_{\text{Imag}}) \exp(i\tilde{S}x_-\cos\theta) \left\{ \prod_{m\neq j}^{n-1} \frac{1}{2\kappa_m} [x_-(\cos\theta + 1) + i2(\kappa_j - \kappa_m)]^{1/2} [x_-(\cos\theta - 1) + i2(\kappa_j - \kappa_m)]^{1/2} \right\}^{-1} \quad (17)$$

Computations were done for both $n = 49$ and $n = 71$ with the use of subroutine DBLINT.[19] The upper limit of x_- was set to 500, which proved to be sufficiently large from earlier calculations (see Figure 5). The distributions are displayed in Figure 6. In analogy with elliptical configurations, circular chains are more compact disks than are linear chains. The quantities $^*\tilde{S}$ and $\langle\tilde{S}\rangle$ are found to be 0.0255 and 0.0376, respectively, for the linear chain, which are about 30% larger than those for the circular case. The quasi-uniaxial compression leading from the most probable elliptical configurations to disks is observed from both Figure 4a and Table II. For the linear chain, $^*\tilde{S}$(disk) is 0.0255 while $^*\tilde{S}_2$(ellipse) is 0.018, not a large difference. Both quantities differ considerably from $^*\tilde{S}_1$(0.048) for the major axis of the most probable ellipse. Configuration parameters pertaining to both circular and linear chains are listed in Table II. The empirical normalization constant appears to depend strongly on the structure of the chain and rather weakly on the chain length.

Disk configurations for linear chains are more compact than are the elliptical configurations. For disks the mean squared radius of gyration $\langle\tilde{s}^2\rangle = 2\langle\tilde{S}\rangle$ is found to be 0.0752, which is only 45% of that for ellipses.

Discussion

As observed from Figures 1–4, the shape distribution functions of 2-dimensional configurations are highly asymmetric. The distributions are skewed along the $\tilde{S}_1$ axis, and once beyond the highly probable values of $\tilde{S}_2$,

they decay very rapidly in the direction of increasing and decreasing $\tilde{S}_2$. The molecules are thus shown to be highly anisometric.

It is also clear from Figures 2b and 4b that the most probable configurations for both circular and linear chains are very compact. Circular chains are likely to have smaller dimensions than linear ones. For example, the principal components of the gyration tensor for circular chains are 70% and 83% of those for linear chains at the most probable configuration of each. For disks, the most probable configuration for the circular chain is 80% as large as that for the linear chain. In the highly extended region, the circular chain is shown to be wider than the linear. For the most probable configurations, the ratio of the two principal components for the linear chains is found to be 2.66:1. It is of interest to compare this result with averaged dimensions found by Šolc[4] for Monte Carlo generated lattice chains. In this case, it was found that $\langle S_1\rangle:\langle S_2\rangle:\langle S_3\rangle \simeq 11.7:2.7:1$. The close similarity between the ratio of most probable components for the two-dimensional linear chain and the two smaller averaged components for the three-dimensional one suggests that their distribution functions behave similarly and that fluctuations for three-dimensional chains will also be quasi-uniaxial.

The distribution function of the gyration tensor varies rapidly with the chain length for short chains, but it reaches the large n limit quickly. In two dimensions, chains with $n = 49$ beads are virtually at the asymptotic $n \to \infty$ limit.

Acknowledgment. This work was supported by the Department of Energy, Grant DE-FG06-84ER45123.

References and Notes

(1) Fixman, M. *J. Chem. Phys.* **1962**, *36*, 306.
(2) Fujita, H.; Norisuye, T. *J. Chem. Phys.* **1970**, *52*, 1115.
(3) Gupta, S. K.; Forsman, W. C. *J. Chem. Phys.* **1976**, *65*, 201.
(4) Šolc, K. *J. Chem. Phys.* **1971**, *55*, 335.
(5) Mattice, W. *Macromolecules* **1981**, *14*, 863.
(6) Rubin, R. J.; Mazur, J. *Macromolecules* **1977**, *10*, 139.
(7) Theodorou, D. N.; Suter, U. W. *Macromolecules* **1985**, *18*, 1206.
(8) Eichinger, B. E. *Macromolecules* **1985**, *18*, 211.
(9) Šolc, K. *Macromolecules* **1972**, *5*, 705.
(10) Šolc, K.; Gobush, W. *Macromolecules* **1974**, *7*, 814.
(11) Eichinger, B. E *Pure Appl. Chem.* **1975**, *43*, 97.
(12) Eichinger, B. E. *Macromolecules* **1977**, *10*, 671.
(13) Neuburger, N. A.; Eichinger, B. E. *J. Chem. Phys.* **1985**, *83*, 884.
(14) Eichinger, B. E. *Macromolecules* **1980**, *13*, 1.
(15) "The IMSL Library", Reference Manual, 9th ed.; International Mathematical and Statistical Libraries: Houston, TX, 1982; Program DCADRE.
(16) Ahlfors, L. V. "Complex Analysis", 3rd ed.; McGraw-Hill: New York, 1979; Chapter 3.
(17) Abramowitz, M.; Stegun, I. A. "Handbook of Mathematical Functions"; National Bureau of Standards, Applied Math. Sec. 55, 1970, p 879.
(18) Eichinger, B. E.; Martin, J. E. *J. Chem. Phys.* **1978**, *69*, 4588.
(19) Gerald, C. F. "Applied Numerical Analysis", 2nd ed.; Addison Wesley: Readings, MA, 1977, Chapter 4.

Excluded Volume Change Due to Segmental Orientation in Polymer Solutions

A. Sariban

Institut für Physik der Universität Mainz, D-6500 Mainz, Federal Republic of Germany.
Received June 26, 1985

ABSTRACT: The excluded volume effect of macromolecules in the external field, producing a partial orientation of segments, was estimated by a model calculation. The lattice model with non-self-intersections of the monomers and with the interactions between the nearest-neighbor monomers was used. The calculations predict maxima of excluded volume in unoriented systems and a continuous decrease of excluded volume with increase of any kind of segment orientation.

Introduction

When the behavior of macromolecules in dilute solution is studied, the Θ-state, where the repulsive and attractive parts of long-range interactions compensate each other and effectively only short-range interactions between two segments remain, is of great importance. The long-range interaction is described in terms of the "excluded volume" for the statistical segment (v_s) or for the monomer (v_m). At the Θ-point, $v_s = v_m = 0$; i.e., excluded volume effects disappear.[1,2]

Recently, Lindner and Oberthür[3] studied the statistical behavior of the isolated macromolecule in shear gradient by means of neutron scattering. The characteristics of the investigated polymer were measured in the Θ-state of the chosen system. The question as to whether the Θ-state determined in the usual manner for the motionless case remains relevant in a shear gradient initiated this work.

It is only possible to obtain the excluded volume in analytical form for simple rigid bodies such as a sphere, cube, or circular cylinder (see, for example, ref 4, Chapter 5, Table 5.1). For the dumbell model,[5] a rigid body that can be considered a first step toward a "pearl necklace" model of a macromolecule, it is possible to obtain the result only in numerical form. If we are interested not only in a rigid body model with a hard-core potential of interactions but also in the attractive interactions of van der Waals type, the task becomes much more difficult. In the present work we have therefore chosen a very simple model that nevertheless contains all the properties of interest in a simplified form. With the aid of this model we hope to attain qualitatively a general understanding of the influence of the (macro)molecular orientation on the excluded volume effects.

Description of the Model

Our macromolecular model is schematically represented in Figure 1. The infinite macromolecule is placed on the simple cubic lattice. The length of each elementary cell

0024-9297/86/2219-0843$01.50/0